Sumamps Gain Maps

J. Posson-Brown, V. Kashyap

March 2009

Abstract

1 Introduction

The gain of the HRC-I has declined since launch (Posson-Brown & Donnelly 2003, Posson-Brown & Kashyap 2007). To address this gain decline, we made a series of time-dependent gain correction maps, which were released in CALDB 3.3.0 (Posson-Brown & Kashyap 2007). In this memo we describe the creation of a new set of time-dependent gain maps. This set is differs from the previous one in two ways. First, the maps are based on scaled SUMAMPS instead of PHA. Second, we model the time-dependence of the gain decline with an exponential plus linear function instead of a pure linear function. In Section 2 we review the observations used to create the maps and our data processing steps. We introduce scaled sumamps in Section 3. The gain correction process is described in Section 4. First, in Section 4.1, we describe the creation of the initial SAMP gain map from pre-flight lab data. Next, we review the corrections for the spatial gain variations (Section 4.2), which are similar to those for the previous set of maps. Finally, we show the exponential plus linear fit to the time-dependent decline (Section 4.3). In Section 4.4 we test the new gain maps on observations of HZ 43, G21.5-0.9, and Cas A (in addition to AR Lac). We summarize in Section 5.

2 Observations and Data Reduction

Yearly calibration observations of AR Lac (Table 1) are taken at 21 locations on the detector to monitor the gain response of the HRC-I. The locations of the pointings are shown in Figure 1. Each observation is nominally 1 ks long; however, effective observation times may be shorter because of background flares. The ObsIDs for all observations used in the analysis presented here are listed in Table 2, along with the deadtime and effective (post-filtering) exposure time.

Our data processing methods are described in detail in Posson-Brown & Kashyap (2007). We will briefly review them here. We reduce the data with CIAO (v?; CALDB ?) and analyze the data with pre-packaged and custom-built IDL routines (e.g., `PINTofALE`; Kashyap & Drake 2000). For each obsid, we reprocess the Level 1 event list with `hrc_process_events` using the newest calibration products and no gain correction (`gainfile=NONE`). We filter on the default GTI and also exclude times when the detector-wide event rate exceeds 150 ct s^{-1} (safely under the telemetry saturation limit of 184 ct s^{-1}).[1]

[1] For the Oct 99 observations done in conjunction with the HRC-I voltage adjustment, we use a set of GTIs based on when the voltage was stable at the low setting (Juda, private communication) in place of the default GTIs.

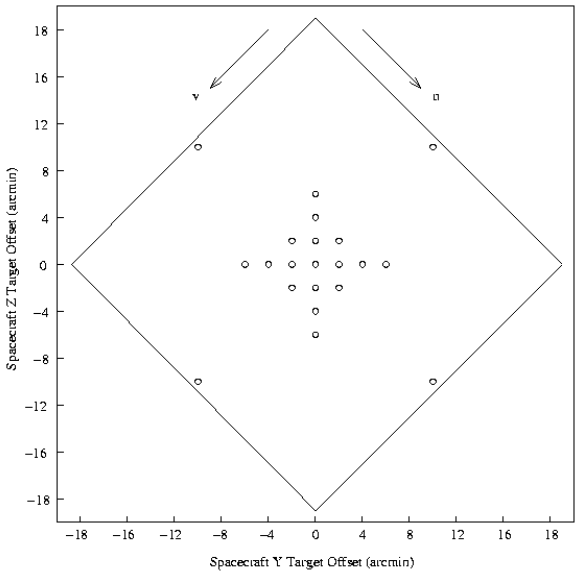

Figure 1: Locations of AR Lac observations on the HRC-I. Calibration observations are carried out at the aimpoint and 20 offset locations each cycle in order to monitor the gain: $(Y_{\rm sim}, Z_{\rm sim})$ = $(0', 0'), (0', \pm 2'), (\pm 2', 0'), (\pm 2', \pm 2'), (0', \pm 4'), (\pm 4', 0'), (0', \pm 6'), (\pm 6', 0')$, and $(\pm 10', \pm 10')$

Table 1: AR Lac stellar parameters

Parameter	**Value**
Other Names	HR 8448 / HD 210334 / RX J2208.6+4544 / HIP 109303
$(\mathrm{RA,Dec})_{ICRS2000.0}$	(22:08:40.818, +45:44:32.12)
$m_{\rm V}, B-V$	6.13, 0.72
Distance	$42-47$ pc
Spectral Type	G2IV/K0IV (RS CVn)
$M_{\rm V}$	3.5/3.3
Masses	1.3/1.3 $M_\odot$
Radii	1.8/3.1 $R_\odot$
Ephemeris	1.98316^d ; conjunction @ 2445611.6290 HJD

We extract source events from an 800x800 box centered on the nominal observation location in chip coordinates. Background is estimated by collecting the events in the *same location*, but from the 20 other observations carried out in that cycle. The background counts thus accumulated are normalized by their appropriate exposure times prior to subtracting them from the counts accumulated at the source location. For the previous set of gain maps (Posson-Brown & Kashyap 2007) we calculated the median PHA value for each observation. Here, we use the mean scaled SUMAMPS value. (We define scaled SUMAMPS in the next section.)

3 Scaled Sumamps

The nominal gain metric for the HRC is Pulse Height Amplitude (PHA), which is the sum of all detector amplifier signals. However, on the HRC-S, PHAs vary largely over small spatial scales

on the detector, while an alternate metric, SUMAMPS, show much less spatial variation (Wargelin 2008). The SUMAMPS value for an event is the sum of the signals from the three amplifiers nearest the event signal on each axis (i.e. AU1, AU2, AU3, and AV1, AV2, AV3) and is given in the Level 1 event list.[2]

Due to the superiority of SUMAMPS for gain measurements on the HRC-S, the HRC calibration team decided to switch from PHA to scaled SUMAMPS ("SAMP") as the standard gain measure. The scaling is done by the amplifier scale factor value (AMP_SF) as follows:

$$SAMP = \frac{SUMAMP \times 2^{AMP\_SF-1}}{C} \tag{1}$$

where C is a constant. For the HRC-S, $C = 128$ (Wargelin 2008). For the HRC-I, we chose $C = 148$. This value was chosen so that the resulting SAMPs would match PHA values closely. Figure 2 shows the SAMP and PHA profiles for an observation of AR Lac done at the aimpoint of the HRC-I. Note that the profiles are very similar but for channel 255. PHA is restricted to 256 channels (0 - 255), so high energy events (mostly background) pile-up in channel 255. However, we have allowed for 512 SAMP channels, so there is no pile-up. For the HRC-I, this is the only significant difference between SAMP and PHA. (Unlike the HRC-S, neither gain metric shows strong small-scale spatial varations.)

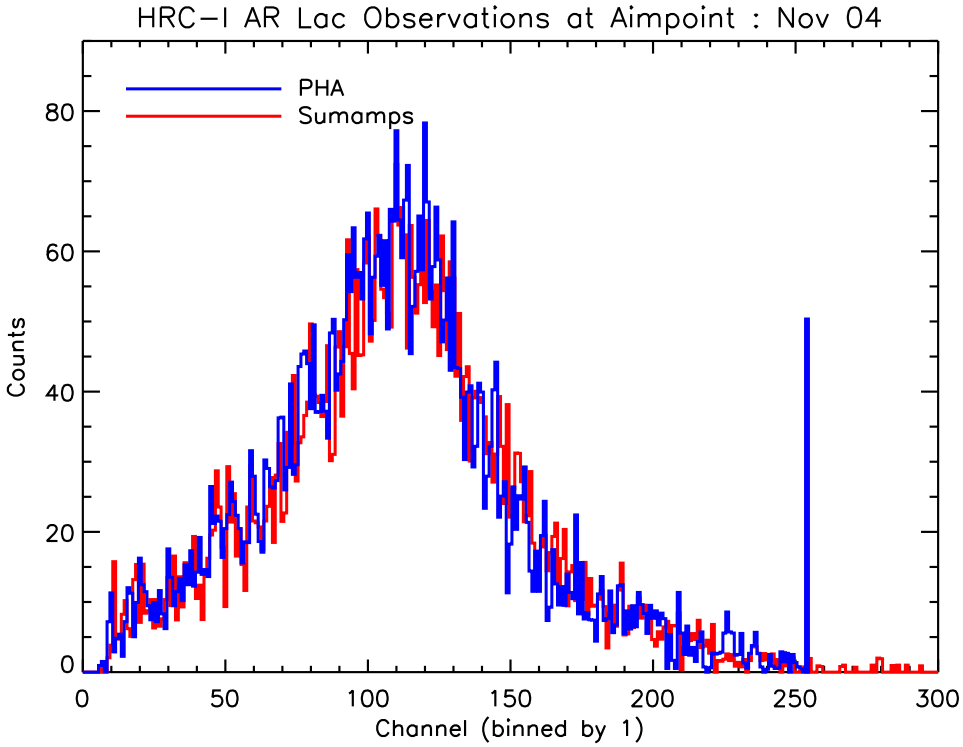

Figure 2: A comparison of PHA and SAMP profiles for HRC-I AR Lac Obsid 04294. Note that the profiles are very similar, except for PHA piling up at channel 255.

Figure 3 shows a scatter plot of mean PHA versus mean SAMP values for HRC-I/LETG obserervations of HR1099, PKS2155-304, and Cygnus X-2. Each data point shows the mean of the

[2]Note that the values of AU3 and AV3 in the Level 1 event list are *not* tap-ringing corrected. However, SUMAMPS in the Level 1 event list is calculated with the tap-ringing corrected values of AU3 and AV3.

total background-subtracted PHA or SAMP profile for events in a given wavelength bin. (The wavelength bins are nonuniform in size and were set so that each contains at least 2000 counts.) The solid blue line shows a linear fit to the data between PHA=140:160. Note that the best-fit slope is nearly one and the best-fit offset nearly zero, indicating that the mean SAMP tracks the mean PHA over a range of energies.

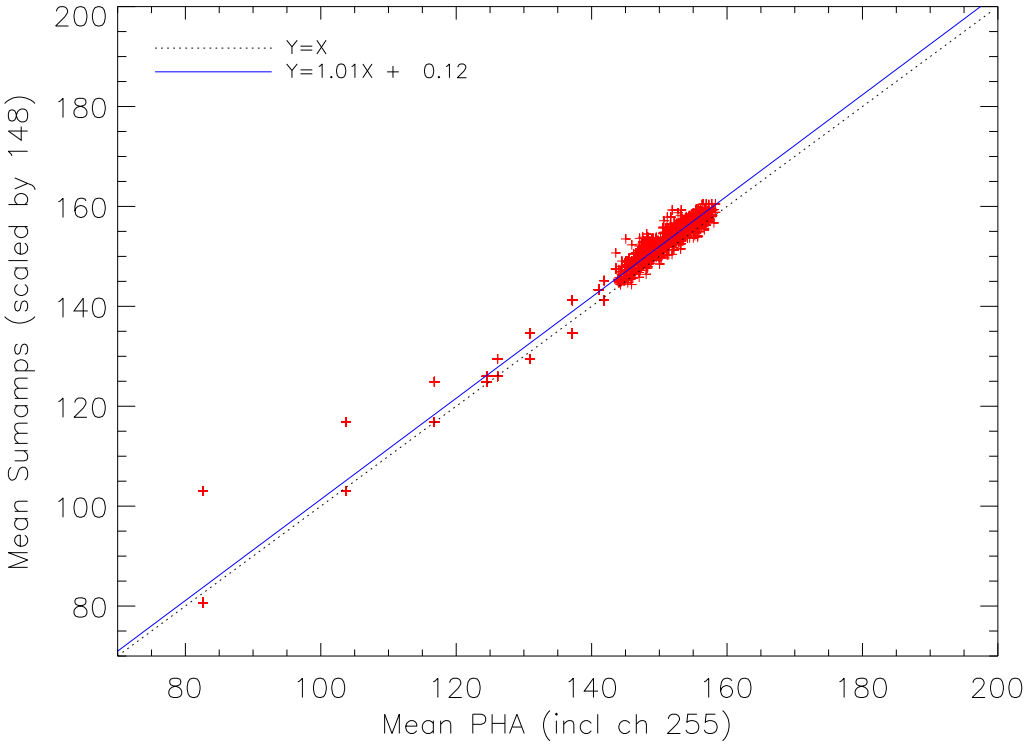

Figure 3: Mean PHA vs mean SAMP for several sources (HR1099, PKS2155-304, and Cygnus X-2) observed with HRC-I/LETG. Each point represents the background-subtracted mean of the combined profile in a given wavelength bin. The nonuniform wavelength bins are such that each been contains at least 2000 counts. The dotted black line is mean SAMP = mean PHA. The solid blue line shows a linear fit to the data between PHA=140:160. Note that the best-fit slope ≈ 1 and the best-fit offset ≈ 0, indicating that the mean SAMP tracks the mean PHA over a range of energies.

Finally, Figure 4 shows the ratio of mean SAMP to mean PHA for the AR Lac observations used to construct the time-dependent gain maps. Note that the mean SAMP and mean PHA are equal to within roughly $\pm 5\%$.

Since the SAMP and PHA values are so similar for the HRC-I, it is not surprising that, like PHA, the SAMP values reveal the decline in gain that has occured since launch. Figure 5 shows the mean SAMP values for all 21 observation locations on the detector, with different plotting symbols for each AO. At all locations, the mean is declining with time. This is nearly identical to what we see with PHA (e.g. Figure 2 in Posson-Brown & Kashyap 2007).

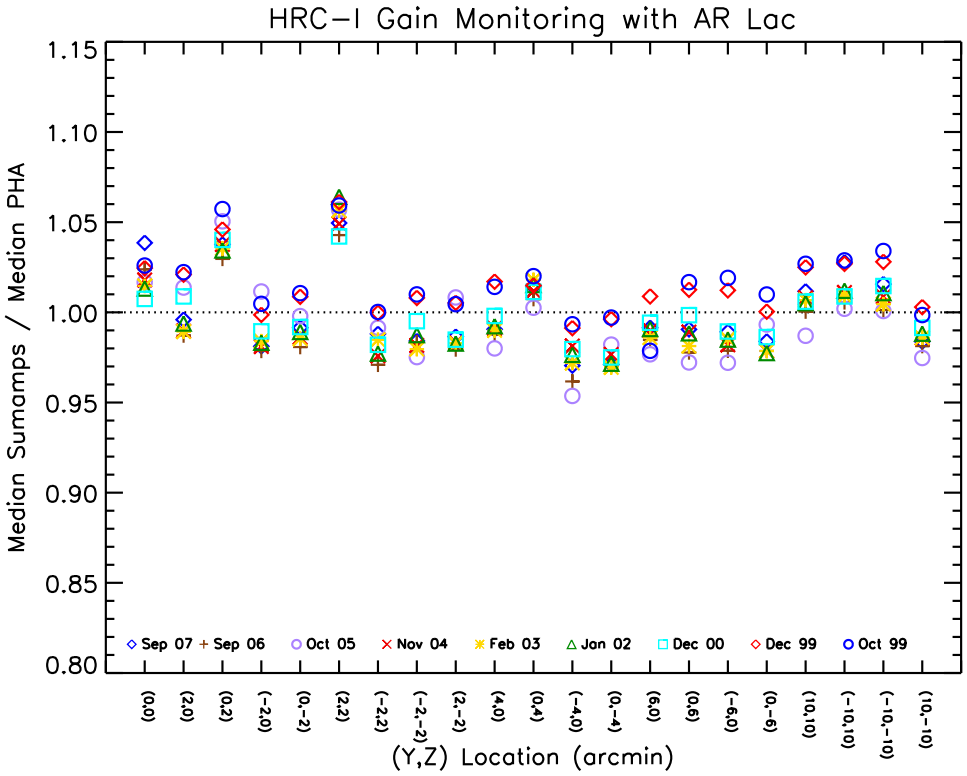

Figure 4: Ratio of mean SAMP to mean PHA for all AR Lac observations.

4 Time Dependent Gain Correction

In order to calculate time-independent SAMP pulse invariant (SPI) values, we carry out corrections to SAMP in two stages, computing the spatial and temporal gain corrections independently as we did previously for the PHA maps (Posson-Brown & Kashyap 2007).

At each observation epoch, the SAMP are multiplied by a non-linear gain correction surface $g(\vec{\mathbf{x}}|t)$ that carries out a "flat-fielding" of the SAMP values, i.e., at each epoch the SAMP at location $\vec{\mathbf{x}}$ are transformed to what the SAMP are at the aimpoint location. After this "flat-fielding", the SAMP are no longer a function of $\vec{\mathbf{x}}$, and thus will be denoted SAMP($\vec{\mathbf{0}}$|t). A time dependent correction, TC(t) is then applied to SAMP($\vec{\mathbf{0}}$|t) to transform them to pulse-invariant SAMP (SPI).

Thus,

$$\mathrm{SPI} = \mathrm{SAMP}(\vec{\mathbf{x}}, t) \times g(\vec{\mathbf{x}}|t) \times TC(t) \equiv \mathrm{SAMP}(\vec{\mathbf{0}}|t) \times TC(t) \tag{2}$$

4.1 Lab Map

The HRC-I gain response was measured during pre-flight ground calibration with a series of flat field maps at six energies spanning 183−6404 eV. For each energy, we create a SAMP gain map by calculating the mean SAMP for events in half-tap (128 x 128 physical pixel) bins. We average these six maps, then normalize the resulting map to its mean central value (calculated from the central 10x10 image pixels). Finally, we take the reciprical of this map, since the gain correction is applied as a multaplicative factor in `hrc_process_events`. This "pre-flight" map, $g_{\mathrm{LAB}}(\vec{\mathbf{x}})$, is shown in Figure 6.

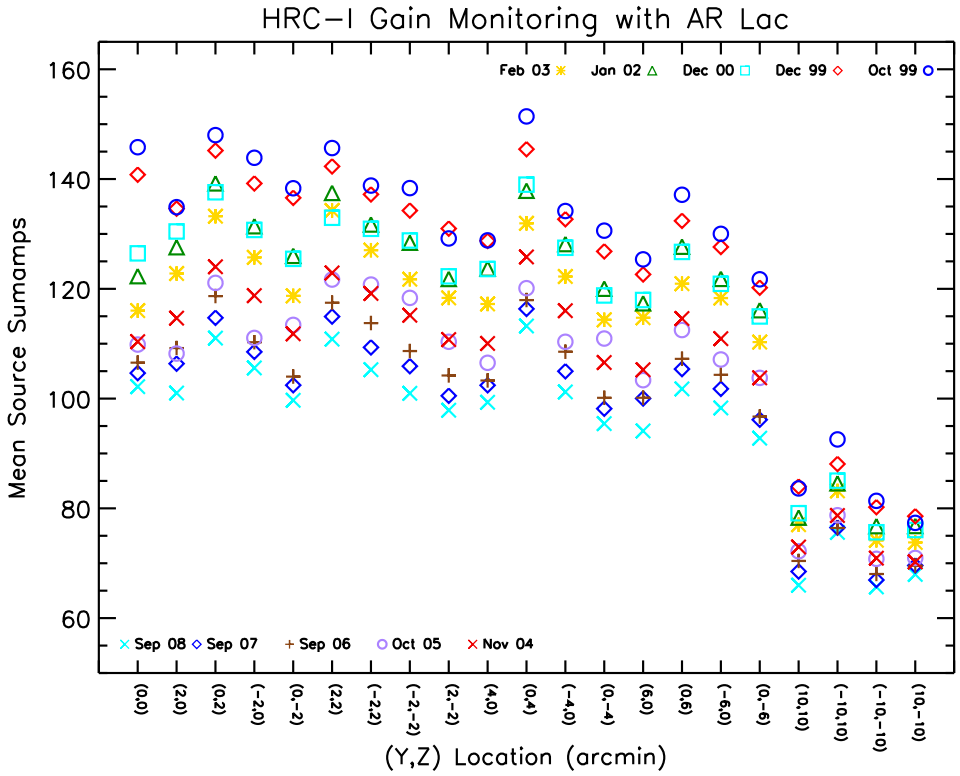

Figure 5: Mean source SAMP as a function of observation location, with different plotting symbols showing different AO's. Note that at all locations, the mean declines with time.

4.2 Spatial Corrections

We correct for the spatial variations in gain response by creating a series correction maps $g(\vec{x}|t)$, one from each AO. We compute them as modifications of the high-resolution lab gain correction map $g_{LAB}(\vec{x})$, described in the previous section. At each of the 21 observation locations, a corrective factor γ is determined. A smooth surface is fit to these corrective factors, and the gain correction map at that epoch is derived as

$$g(\vec{x}|t) = g_{LAB}(\vec{x}) \times \gamma(\vec{x}|t) \tag{3}$$

This procedure preserves the high spatial-frequency information present in the lab calibration data, while accounting for the gross changes that have occurred in the gain since launch.

The corrective factors γ are computed by a direct comparison of the spectra at different pointings to the aimpoint spectrum. This method was describe in detail in Posson-Brown & Kashyap (2007), but we will review it briefly here.

First, putative spatially gain-corrected SAMPs are computed as

$$\mathrm{SAMP}_{LAB}(\vec{x},t) = \mathrm{SAMP}(\vec{x},t) \cdot g_{LAB}(\vec{x}). \tag{4}$$

These modified SAMPs are binned into spectra $f(SAMP)$, and the best-fit value of γ that results in the best match between $f(\gamma \cdot \mathrm{SAMP}_{LAB}(\vec{x},t))$ and $f(\mathrm{PHA}_{LAB}(\mathrm{aim},t))$ is determined via a grid-search over γ that minimizes the χ^2 value between the two functions.

The resulting correction factors are shown in Figure 7. We use them to interpolate a minimum curvature surface at all locations over the detector to obtain the corrective surface $\gamma(\vec{x}|t)$. This is

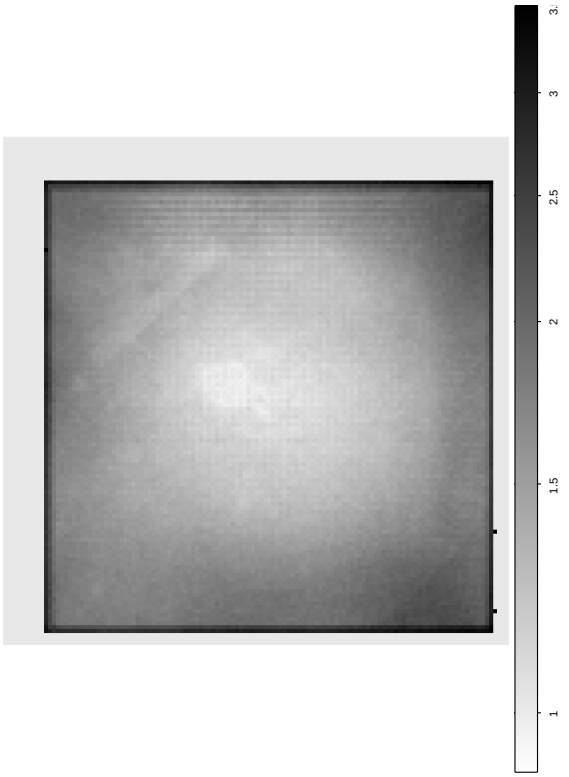

Figure 6: Pre-flight SAMP gain map.

multiplied by the high-resolution gain map $g_{LAB}(\vec{\mathbf{x}})$ to obtain the gain correction map $g(\vec{\mathbf{x}}|t)$ for the epoch (Equation 3).

We test the spatial gain correction maps by independently applying $g(\vec{\mathbf{x}}|t)$ to the SAMP($\vec{\mathbf{x}}$,t) values and comparing the *mean*(SAMP($\vec{\mathbf{0}}|t$)) for all the datasets. The results are shown in Figure 8. As expected, the medians for each epoch are uniform, i.e., the gain correction has removed the spatial dependence in the SAMP($\vec{\mathbf{x}}$,t). Note that these maps are intermediate products, and are *not* distributed within the calibration database.

4.3 Temporal Correction

Having made correction maps for the spatial non-uniformity of the detector response, our next task is to correct for the time-dependence in the gain decline. As described above, we seek to calculate the correction as a function of time only, and then correct the gain correction maps from each epoch ($g(\vec{\mathbf{x}}|t)$, see §4.2) by multiplying with this factor (see Equation 2). That is, we want to find a temporal correction factor (TC) such that

$$SPI = \text{SAMP}(\vec{\mathbf{0}}|t) \times TC(t), \tag{5}$$

where t is the time since October 1999, and *SPI* is the spatially and temporally invariant SAMP, and SAMP($\vec{\mathbf{0}}|t$) are the "flat-field" SAMP values.

For these previous set of maps, we fit the PHAs with a simple linear function, excluding the first two data points from the fit (see Figure 3 in Posson-Brown & Kashayp 2007). However, we now fit the SAMPs with an exponential plus linear function, i.e.

$$mean(\text{SAMP}(\vec{\mathbf{0}}|t)) = a_0 e^{-a_1 t} + a_2 t + a_3. \tag{6}$$

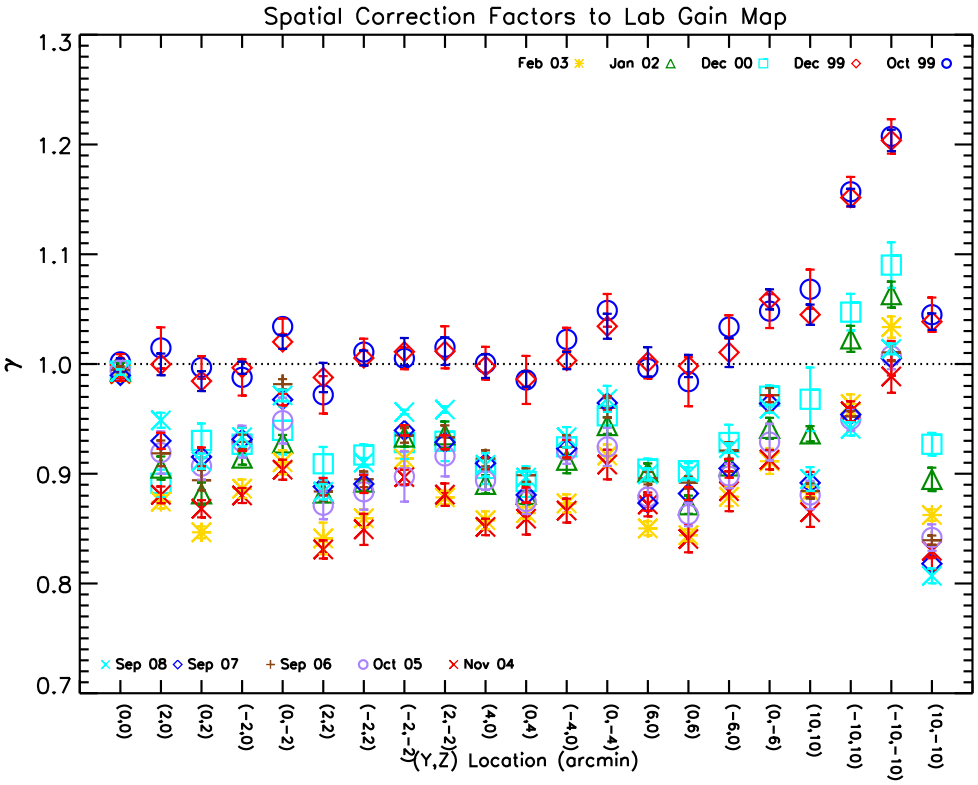

Figure 7: Spatial gain correction factors, relative to the aimpoint, for each AO.

We find best-fit parameters of $a_0 = 26.22$, $a_1 = 7.09 \times 10^{-2}$, $a_2 = -1.96 \times 10^{-1}$, and $a_3 = 122.16$. This fit is shown in Figure 9.

Our time correction is then the reciprocal of this normalized fit, i.e.

$$TC(\mathrm{t}) = \frac{a_0 + a_3}{a_0 e^{-a_1 t} + a_2 t + a_3}. \tag{7}$$

This time correction is show in Figure 10 as the dotted line. The time correction for the previous set of maps, derived from a strictly linear fit excluding the first two data points, is shown by the dashed line. Note that the new time correction, from the exponential plus linear fit, is continuous at time=0, whereas the previous time correction jumps from 1 at time=0 to 1.12. ($TC(0) = 1$ by definition.)

For each epoch of observation t, we obtain the corresponding correction factor $TC(\mathrm{t})$, and multiply the previously derived "flat-fielded" gain maps $\mathrm{g}(\vec{\mathbf{x}}|\mathrm{t})$ to obtain the gain correction map at each epoch. These maps, one for each epochs, are the final product of our analysis. They will be released in the CALDB once `hrc_process_events` and related CIAO tools have been modified to use SAMP and SPI in place of PHA and PI.

4.4 Testing the New Maps

To test the new gain-correction maps, we return to the raw source and background SAMP values calculated from the AR Lac Level 1 event lists. We convert the values to SPI using the appropriate map, then find the mean background subtracted SPI. Figure 11 shows the median PI values for each AO as a function of observation location on the detector. Comparing this figure to raw SAMPs

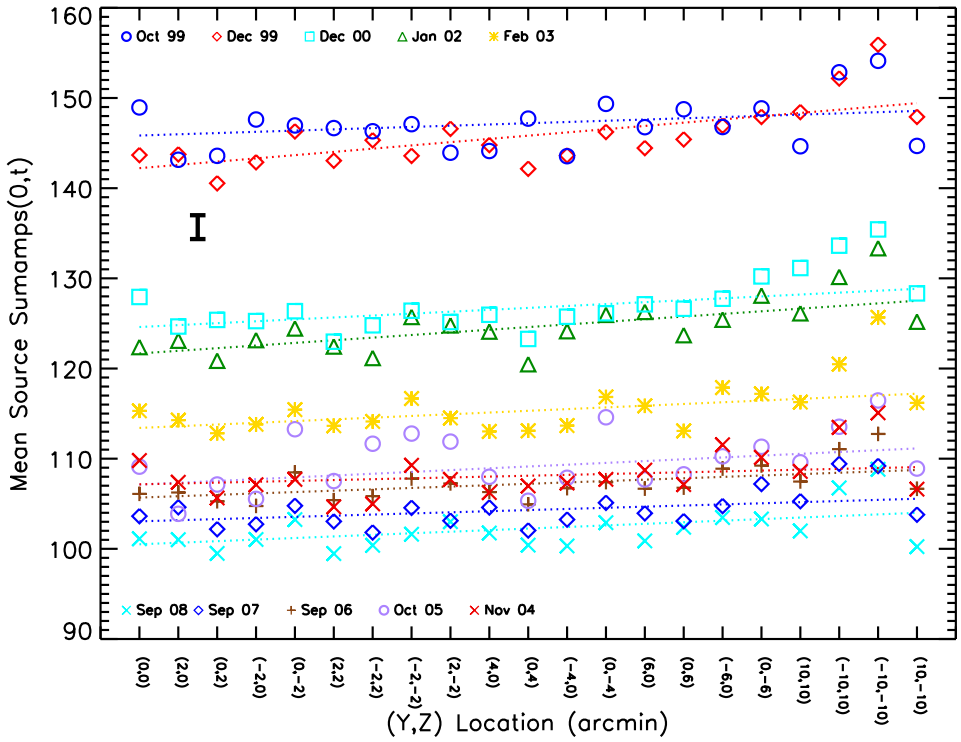

Figure 8: Mean “flat-fielded” SAMP values as a function of location on the detector, for all the AR Lacobservations. The dashed lines show the best-fit line to each set.

versus location (Figure 5) and spatially-corrected SAMPs versus location (Figure 8), we can see that the new gain correction maps have performed their task: the spatial and temporal dependencies from pulse-height values have been removed.

5 Summary

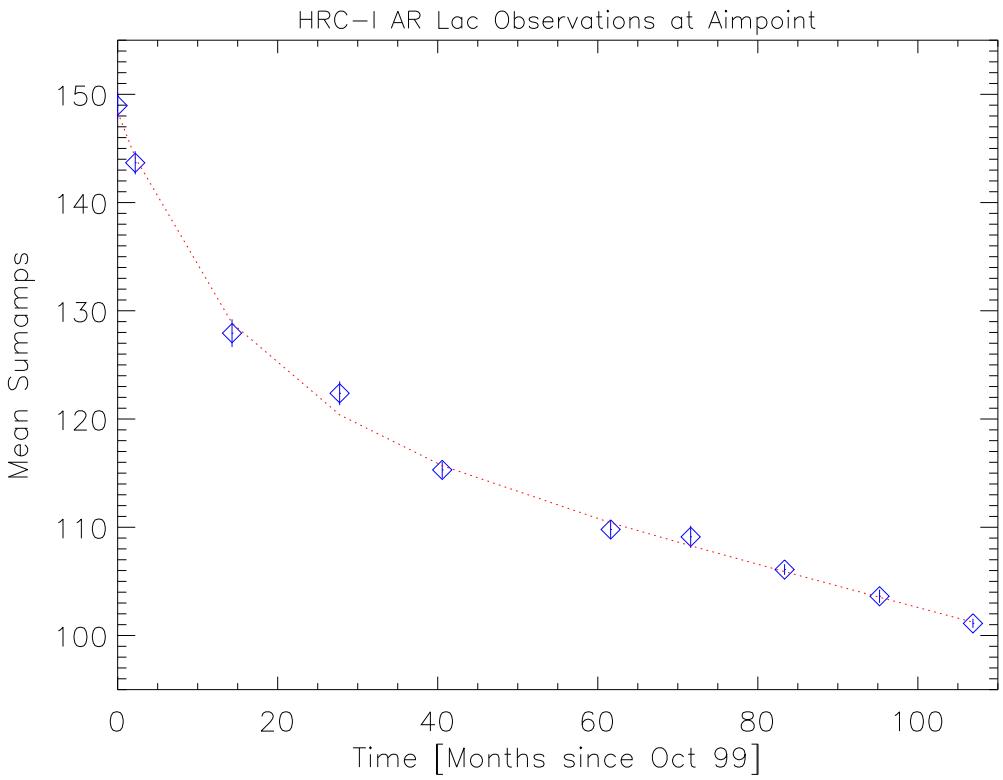

Figure 9: Exponential plus linear fit to mean SAMP at the aimpoint. The reduced χ^2 value is 1.18.

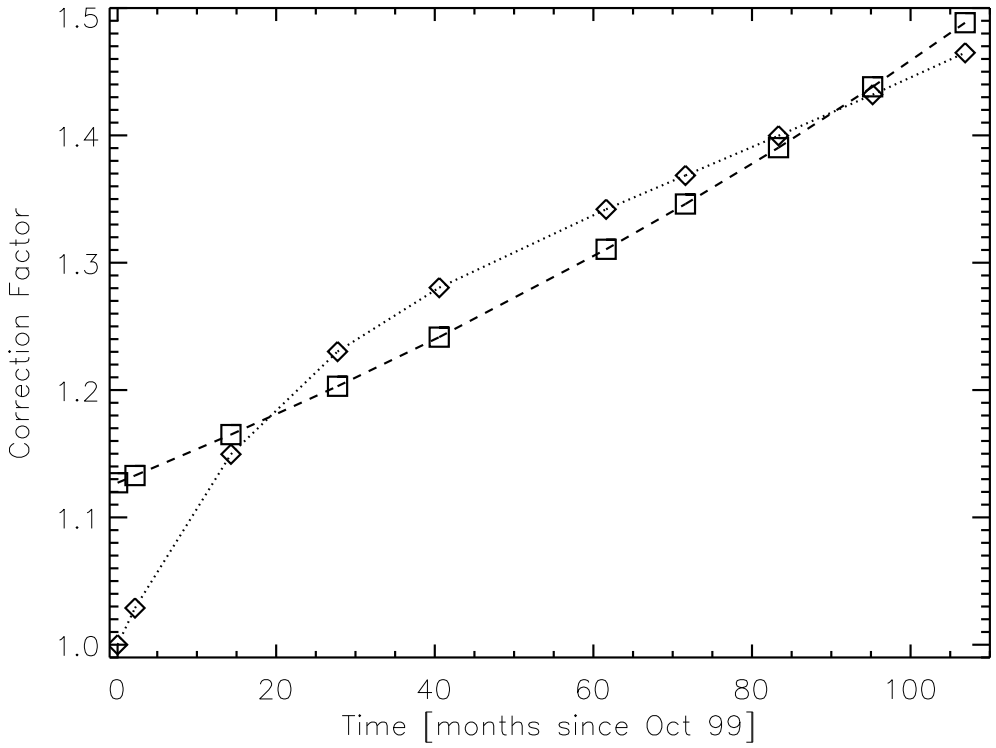

Figure 10: Comparison of old and new time correction functions. The new function, show as a dotted line, is based on an exponential plus linear fit to the aimpoint SAMPs. The previous correction (dashed line) was based on a linear fit to aimpoint PHAs.

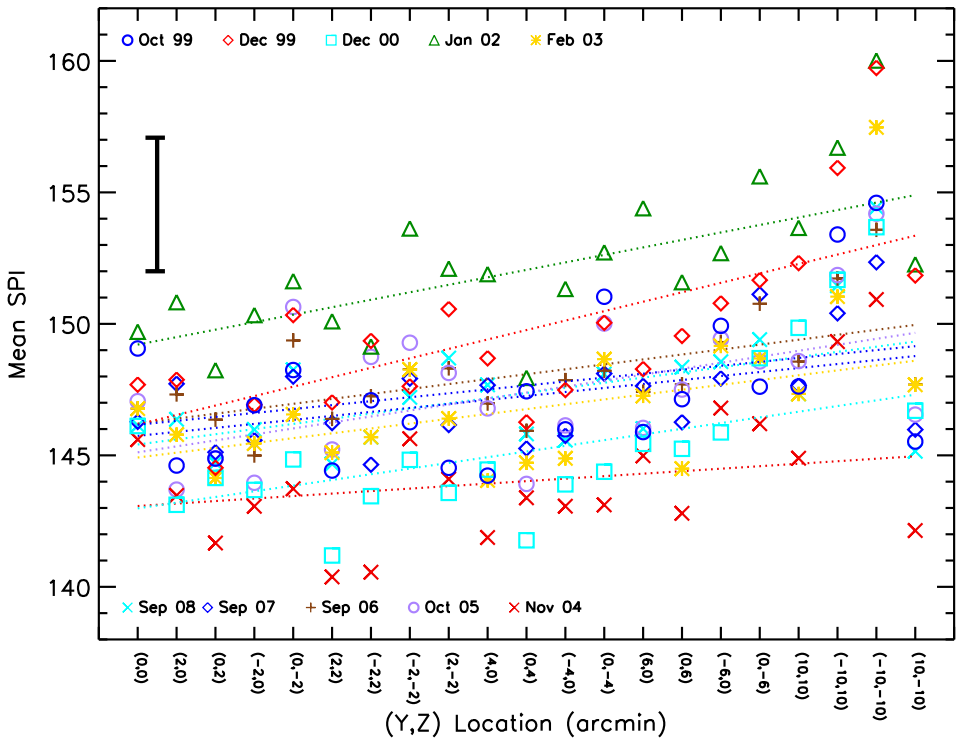

Figure 11: Mean SPI values for AR Lac.

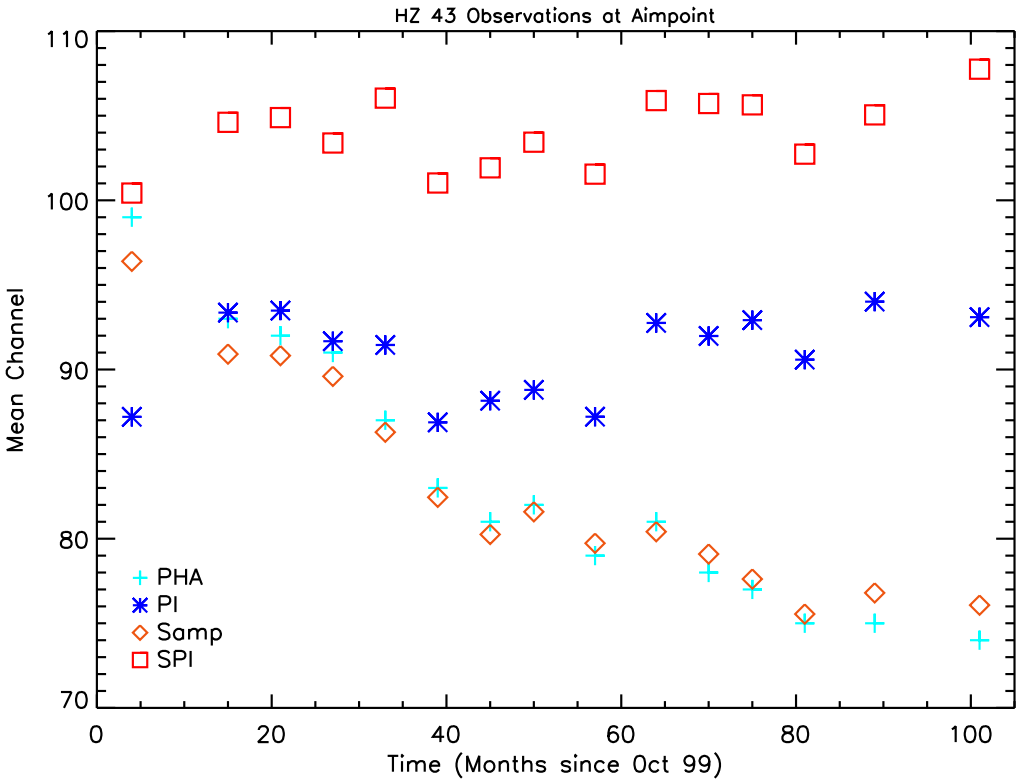

Figure 12: Mean SPI values for HZ 43 (red boxes), compared to mean SAMP values (orange diamonds), mean PHA (cyan crosses), and mean PI (blue asterisks). As expected, mean SAMP closely tracks mean PHA.

References

– Juda M 2001, *HRC Rates and High Solar Activity* (CXC Memo, available at `http://hea-www.harvard.edu/ juda/memos/hrc_bkg/high_solar.html`

– Juda M, Donnelly R H, Hole K T, Kenter A T, Kraft R P, Murray S S, Pease D O, Wilton C and Zombeck M V 2002, Proceedings of SPIE, 4851, 112

– Juda M 2004, *HRC-Y Shutter Failure (OCCcm06110): FDB Closeout*, Chandra Flight Note (#441), available at `http://hea-www.harvard.edu/ juda/memos/shutter_anomaly/shutter_failure.pdf`

– Kashyap V and Drake J J 2000, BASI 28, 475

– Pease D and Drake J 2003, *Monitoring the HRC-S Gain with the LETG/HRC-S* (CXC Memo, available at `http://asc.harvard.edu/cal/Hrc/gain.html`

– Posson-Brown J and Donnelly R H 2003, *Evolution of PHA Response in the HRC,* (CXC Memo, available at `http://asc.harvard.edu/cal/Hrc/gain.html`)

– Posson-Brown J and Kashyap V 2007, *HRC-I Gain Correction*, (CXC Memo, available at `http://asc.harvard.edu/cal/Hrc/Documents/Gain/hrci_gain_correction.pdf`)

– van Dyk D A, Connors A, Kashyap V and Siemiginowska A 2001, ApJ, 548, 224

– Wargelin B J, Ratzlaff P W and Juda M 2008 *A New Gain Map and Pulse-Height Filter for the Chandra LETG/HRC-S Spectromter*, (CXC Memo, available at `http://cxc.harvard.edu/cal/Letg/Gain`

– Wilton C, Posson-Brown J, Juda M and Kashyap V 2005 *The HRC-I Gain Map*, Poster #9.10 at the 2005 Chandra Calibration Workshop, available at `http://asc.harvard.edu/ccw/proceedings/05_proc/presentations/wilton/`

Table 2: HRC-I AR Lac calibration observations used in creation of the time-dependent gain correction maps.

(Y, Z) Offset [arcmin]	Oct 99			Dec 99			Dec 00			Jan 02		
	ObsID	Exptime [s]	DTCOR	ObsID	Exptime [s]	DTCOR	ObsID	Exptime [s]	DTCOR	ObsID	Exptime [s]	DTCOR
(0,0)	1321	994.893	0.994	1484	1287.76	0.995	996	3079.97	0.996	2608	1187.59	0.994
(2,0)	1324	994.911	0.995	1485	1279.25	0.994	2345	1182.04	0.988	2617	1186.43	0.994
(0,2)	1342	994.932	0.995	1491	1288.67	0.995	2351	1180.02	0.995	2611	1186.41	0.994
(-2,0)	1336	992.810	0.994	1489	1293.24	0.998	2349	1184.09	0.995	2610	1193.82	0.994
(0,-2)	1330	994.854	0.994	1487	1279.34	0.995	2347	1177.71	0.993	2618	1189.64	0.994
(2,2)	1345	994.893	0.994	1492	1279.76	0.994	2352	1180.02	0.995	2604	1122.47	0.999
(-2,2)	1339	992.794	0.994	1490	1287.82	0.995	2350	1188.19	0.995	2619	1188.50	0.994
(-2,-2)	1333	994.878	0.994	1488	1287.83	0.995	2348	1177.97	0.995	2624	1658.56	0.995
(2,-2)	1327	994.768	0.994	1486	1286.66	0.995	2346	1182.04	0.993	2609	1188.50	0.994
(4,0)	1348	994.927	0.995	1493	1286.80	0.995	2353	1149.96	0.995	2620	1191.83	0.994
(0,4)	1366	994.908	0.995	1499	1286.95	0.995	2359	1189.98	0.995	2606	1197.72	0.994
(-4,0)	1360	994.983	0.995	1497	1286.74	0.995	2357	1189.99	0.995	2621	1186.68	0.994
(0,-4)	1354	994.912	0.995	1495	1288.72	0.995	2355	1177.94	0.995	2612	1193.78	0.994
(6,0)	1351	994.875	0.994	1494	1287.65	0.995	2354	1179.98	0.995	2605	1188.82	0.994
(0,6)	1369	994.901	0.995	1500	1289.40	0.995	2360	1188.90	0.995	2607	1186.77	0.994
(-6,0)	1363	994.946	0.995	1498	1287.84	0.995	2358	1180.00	0.995	2613	1188.64	0.994
(0,-6)	1357	993.032	0.995	1496	1289.85	0.995	2356	1165.67	0.995	2614	1188.62	0.994
(10,10)	1372	994.967	0.995	1501	1288.26	0.995	2361	1189.99	0.995	2615	1186.83	0.995
(-10,10)	1381	8145.72	0.993	1504	1284.88	0.995	2364	1179.96	0.995	2616	1195.73	0.995
(-10,-10)	1378	994.991	0.995	1503	1290.18	0.995	2363	1099.99	0.995	2623	1188.72	0.995
(10,-10)	1375	995.055	0.995	1502	1287.84	0.995	2362	1159.97	0.995	2622	1195.72	0.995
(Y, Z) Offset [arcmin]	**Feb 03**			**Nov 04**			**Oct 05**			**Sep 06**		
	ObsID	**Exptime [s]**	**DTCOR**	**ObsID**	**Exptime [s]**	**DTCOR**	**ObsID**	**Exptime [s]**	**DTCOR**	**ObsID**	**Exptime [s]**	**DTCOR**
(0,0)	4294	1176.86	0.994	6133	1076.92	0.993	5979	1970.90	0.992	6519	3143.17	0.991
(2,0)	4303	1179.68	0.994	6134	1071.80	0.993	5980	1045.48	0.884	6520	1173.98	0.991
(0,2)	4297	1179.68	0.994	6135	1079.14	0.993	5981	589.796	0.500	6521	1171.12	0.991
(-2,0)	4296	1175.69	0.995	5063	1059.93	0.993	5982	1061.43	0.896	6522	1175.34	0.991
(0,-2)	4304	1177.40	0.994	5064	1068.12	0.993	5983	410.867	0.349	6523	1165.13	0.991
(2,2)	4290	646.692	0.999	5066	1077.09	0.993	5985	539.020	0.457	6525	1169.15	0.991
(-2,2)	4305	1100.07	0.994	5067	1083.02	0.993	5986	383.852	0.323	6526	1172.19	0.991
(-2,-2)	4310	1553.98	0.995	5068	1073.57	0.993	5987	235.416	0.200	6527	1159.18	0.991
(2,-2)	4295	1178.42	0.995	5065	1083.07	0.993	5984	582.467	0.493	6524	1165.45	0.991
(4,0)	4306	1175.64	0.995	5071	1066.16	0.992	5990	1125.68	0.992	6530	1164.40	0.991
(0,4)	4293	1178.96	0.994	5073	1068.13	0.992	5992	1171.31	0.993	6532	1175.32	0.991
(-4,0)	4307	1179.66	0.994	5075	511.306	0.992	5994	1174.03	0.993	6534	1174.22	0.991
(0,-4)	4300	1178.63	0.994	5069	1076.88	0.993	5988	311.304	0.264	6528	1174.21	0.991
(6,0)	4291	886.898	0.991	5072	1066.25	0.992	5991	1166.76	0.993	6531	1171.18	0.991
(0,6)	4292	1175.26	0.994	5074	672.529	0.989	5993	1179.36	0.993	6533	1165.43	0.991
(-6,0)	4299	1182.44	0.994	5076	798.618	0.990	5995	1167.47	0.992	6535	1171.12	0.991
(0,-6)	4298	1173.10	0.994	5070	1077.90	0.993	5989	415.781	0.357	6529	1165.94	0.991
(10,10)	4301	1176.34	0.994	5079	1078.81	0.993	5998	1176.88	0.992	6538	1182.17	0.991
(-10,10)	4302	1173.44	0.994	5080	1073.95	0.993	5999	1164.38	0.992	6539	1174.40	0.991
(-10,-10)	4309	1182.73	0.995	5077	1061.77	0.992	5996	1058.72	0.989	6536	1172.21	0.991
(10,-10)	4308	1173.62	0.995	5078	1078.00	0.993	5997	1148.12	0.990	6537	1164.54	0.991